

Confinement and distribution of the composition in semicrystalline/amorphous miscible blends of PEKK/PEI: a calorimetry study

Aude Belguise, Sabine Cantournet, Victor Fabre, Karine Le Gorju, Valérie Gaucher, Jean-François Tahon, Bruno Bresson, Christian Fretigny, François Lequeux, Helene Montes

▶ **To cite this version:**

Aude Belguise, Sabine Cantournet, Victor Fabre, Karine Le Gorju, Valérie Gaucher, et al.. Confinement and distribution of the composition in semicrystalline/amorphous miscible blends of PEKK/PEI: a calorimetry study. Macromolecules, 2021, 54 (16), pp.7364-7376. 10.1021/acs.macromol.1c00344 . hal-03324936

HAL Id: hal-03324936
https://espci.hal.science/hal-03324936

Submitted on 24 Aug 2021

HAL is a multi-disciplinary open access archive for the deposit and dissemination of scientific research documents, whether they are published or not. The documents may come from teaching and research institutions in France or abroad, or from public or private research centers.

L'archive ouverte pluridisciplinaire **HAL**, est destinée au dépôt et à la diffusion de documents scientifiques de niveau recherche, publiés ou non, émanant des établissements d'enseignement et de recherche français ou étrangers, des laboratoires publics ou privés.

Confinement and distribution of the composition in semicrystalline/amorphous miscible blends of PEKK/PEI: a calorimetry study

Aude Belguise[1,2], Sabine Cantournet[2], Victor Fabre[3], Karine Le gorju[3], Valérie Gaucher[4], Jean-François Tahon[4], Bruno Bresson[1], Christian Fretigny[1], François Lequeux[1], Helene Montes[1]*

1 UMR 7615, CNRS, ESPCI Paris, PSL University, Paris, 75 005, France

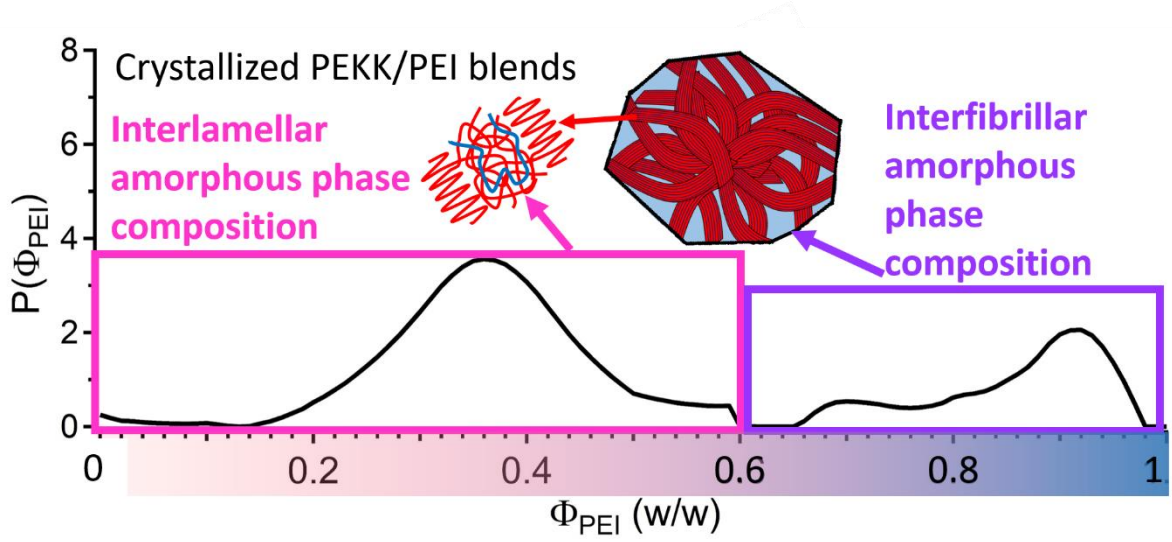
2 Centre des Matériaux, UMR 7633, CNRS, Mines ParisTech, PSL University, Paris, 91003, France

3 Research and Innovation Centre, Hutchinson SA, Chalette-sur-Loing, 45120, France

4 UMET, UMR 8207, CNRS, Univ. Lille, INRAE, Centrale Lille, Lille, 59000, France

*Corresponding author : Helene Montes, email : helene.montes@espci.fr

Table of Content Graphics



ABSTRACT:

By combining SAXS and DSC measurements, we analyse the widening of the glass transition measured for miscible mixtures of semicrystalline PEKK chains and fully amorphous PEI chains. The calorimetric analysis reveals that the amorphous interlamellar phase is subject to confinement effects. In addition, we measure wide composition distributions for the amorphous interlamellar and interfibrillar phases. We quantitatively identify, through a careful analysis of the signals, the fraction and average composition of each amorphous phase and the composition distribution. We conclude that the final distribution of the polymer chains that do not crystallize in the interlamellar and interfibrillar phases results from the crystallization dynamics of the mixtures.

1. INTRODUCTION

Semicrystalline polymers are used by industry for some mechanical parts due to their lower weight than metals. Moreover, the stiffness and ductility of a given polymer material are increased, as the polymer chains have partly crystallized. A method for tuning the properties of

semicrystalline polymers – mainly polyolefin – is to introduce along polymer chains that crystallize a small amount of noncrystallizing monomers[1]. Another method is to use blends of miscible polymers, one crystallizing and the other not. Classical examples are PC/PMMA blends [2, 3], PMMA/PVDF [4-8] and PMMA/PEO blends [9, 10]. This allows tuning of not only the crystallinity but also the glass transition temperature of the sample. The chains of the noncrystallizing polymer are expelled from crystalline lamellae. Therefore, in such a crystallized miscible blend, the amorphous phase is a mixture that coexists with the crystallizing polymer lamellae. However, for these blends, identification of the arrangement of the amorphous/crystalline phases remains challenging.

Even for simple semicrystalline polymers, the existence of three kinds of amorphous phases has been reported [11 - 13]. As illustrated in Figure 1, the crystalline domains may be arranged in spherulites with diameters of a few μm. In this case, a crystallized sample is composed of some spherulites that can be embedded in the first kind of amorphous matrix called the interspherulitic amorphous phase. The second kind of amorphous phase is the so-called interlamellar amorphous phase. This corresponds to chains located in the lamellar stacks between crystalline lamellae. Depending on the thickness of the interlamellar layer, polymer chains can be highly confined in the interlamellar domains, resulting in changes in their dynamics compared to the bulk[14]. Moreover, chains that partly crystallize and are thus involved in both the crystalline and interlamellar domains can be stretched at the interface of the two phases [1, 15]. Lastly, the existence of a third kind of amorphous phase has been deduced by various authors and is called either the inter(lamellar bundle) or interfibrillar amorphous phase [3,16-20]. This phase is expected to consist of amorphous pockets inside spherulites. However, the precise nature of the interfibrillar amorphous phase is not very clear. These three amorphous phases are usually related to distinct length scales: a few nanometers for the interlamellar phase, a few hundreds of nanometers for the interfibrillar phase and a few micrometers for the

interpherulitic amorphous phase [21]. According to these different length scales, chain segments should be confined in the interlamellar phases between crystalline lamellae whereas there should be no confinement effect for chain segments inside interfibrillar and interspherulitic domains.

The arrangement of the three amorphous phases in crystallized miscible blends has been suggested to result from the balance between the crystallization kinetics and the diffusion kinetics of the polymer chains rejected from the crystalline domains [22]. Moreover, each amorphous phase itself may be heterogeneous. Distribution of the composition has been observed in the amorphous phases of crystallized blends [21, 23] and in particular in the system of interest here, PEKK/PEI miscible blends [24].

In this work, combining differential scanning calorimetry (DSC) and small angle X-ray scattering (SAXS) measurements, we demonstrate that in crystallized PEKK/PEI blends, significant composition distributions occur both between interlamellar and interfibrillar phases and inside each kind of amorphous phase. We quantitatively determine the composition distribution in the interlamellar phase in which chain segments are confined and interfibrillar phases in which chain segments are not confined.

Furthermore, we quantitatively identify the effects of confinement and composition distribution on the dynamics of amorphous chains in miscible crystallized PEKK/PEI blends. In the interlamellar amorphous phase corresponding to domains within which chain segments are confined, the effect of confinement on the chain segments dynamics is complex: a large fraction of chains segments with slowed down dynamics coexists with a small fraction of chain segments whose dynamics is slightly accelerated

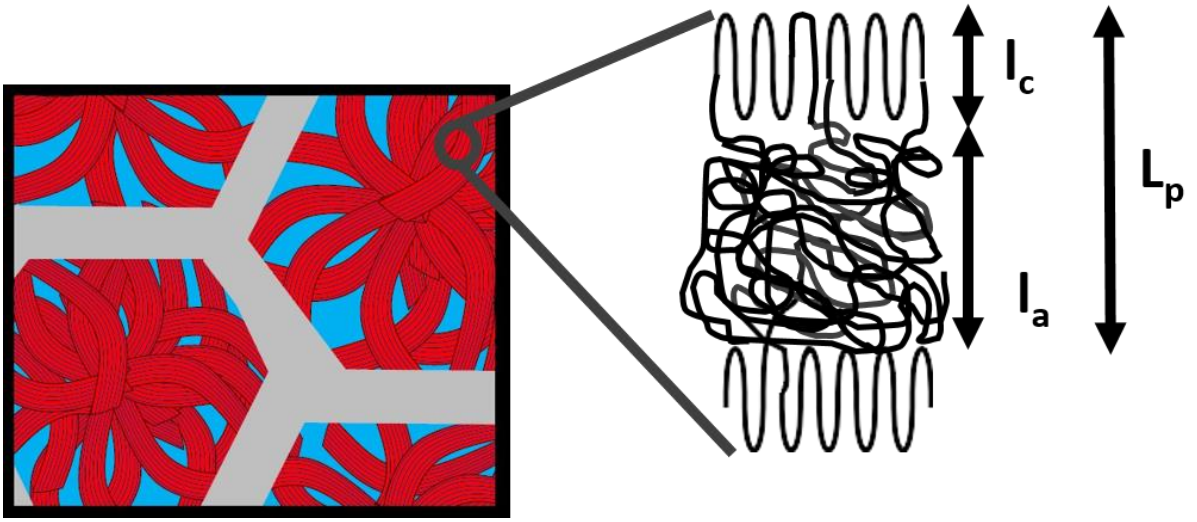


Figure 1: Schematic representation of semicrystalline polymers. Lamellar stacks are in red, the interfibrillar amorphous phase is in blue, and the interspherulitic phase is in grey. The lamellar stacks are made of alternate lamellae of crystallized polymer chains of thickness lc with layer of amorphous polymer chains of thickness l_a. The period length of the lamellar stack is $L_p=l_c+l_a$. The characteristic length of the interfibrillar domains is expected to be large compared to the thickness l_a (few nanometers).

2. MATERIALS AND METHODS

2.1. Materials

PEI chains were provided by Sabic (referenced as PEI Ultem 1010). Their glass transition temperature is approximately 213°C, and their density is reported to be 1.27g/cm^3 [25, 26]. This is a noncrystallizing polymer.

PEI chains were mixed with PEKK chains that can crystallize. In this work, we used PEKK chains with 60% para groups and 40% meta groups supplied by Arkema (PEKK 6003). Their glass transition temperature is approximately 160°C, and their melting temperature is higher than 300°C. PEKK/PEI blends of varying composition were prepared by extrusion at a temperature higher than 300°C. We checked that the extrusion procedure did not change the

molecular weight of polymer chains. The density of 100% amorphous PEKK is 1.27 g/cm^3 [27, 28], and that of the crystalline phase is reported to be approximately 1.4 g/cm^3 [29 - 31].

We chose 60/40 para/meta structure PEKK chains because their crystallization kinetics are slow enough to obtain amorphous samples by simple quenching of macroscopic samples in the melt state at room temperature. Additionally, crystallized samples are easily obtained by annealing between the glass transition temperature and the melting temperature of the blend.

2.2. AFM observations

Crystallized samples were observed at the spherulite scale with atomic force microscopy (AFM).

AFM observations were carried out on the free surface of samples that had been melted at 360°C for 30 min and then crystallized at an isotherm of 250°C until the end of crystallization. AFM images were acquired in tapping mode with a BudgetSensors tapping cantilever with a resonance frequency of 300 kHz and stiffness equal to 40N/m. The scan frequency was 0.5 Hz, and 256 points per line were acquired. The free amplitude was set to 20 nm, and the working amplitude reduction was 0.90. For clarity, we chose to display the amplitude error signal of the image.

2.3. X-ray scattering

The characteristic lengths of crystalline stacks were measured with SAXS. SAXS measurements were realized in transmission mode with Cu Kα radiation (λ = 1.54189 Å). Scattering patterns were collected with a CCD detector. Data were collected for a q range from 7 x 10^{-4} to 0.31 Å^{-1}. Samples were crystallized from the amorphous glassy state with a 250°C isotherm for more than 49 h so that samples with PEI fractions as high as 70% had maximally crystallized. The thickness of the samples was approximately 2 mm. The empty beam, which

was measured in the absence of a sample, was subtracted from scattered signals, which were normalized according to the thickness, measurement time and transmission, resulting in the quantity I_{exp}, which is the sum of the intensity scattered by the polymer materials I(q) and the background intensity I_b. The latter was estimated by fitting for large q the quantity $I_{exp}(q)$ with the form $I_b + \frac{A}{q^4} exp(-sq^2)$, where I_b, A and s are fitting parameters. The intensity scattered by the polymer material I(q) was thus deduced by applying $I(q)=I_{exp}(q)-I_b$.

We have checked that the contrast between amorphous PEKK and PEI chains is small compared to the contrasts between the crystallized PEKK chains and the pure amorphous PEKK or PEKK/PEI mixtures. Therefore, the intensity scattered by our samples results from the contrast between the crystallized and amorphous domains. In order to characterize the lamellar stacks in PEKK/PEI blends, an estimate of the one dimensional correlation function was computed from the intensity scattered by each blend; it is obtained from the Lorentz corrected SAXS intensity [32-33] given by : $Y(r) = \int 4\pi I(q) q^2 cos(2\pi qr) dq$

Figure 2 presents the typical density correlation function Y as a function of the distance r we obtained.

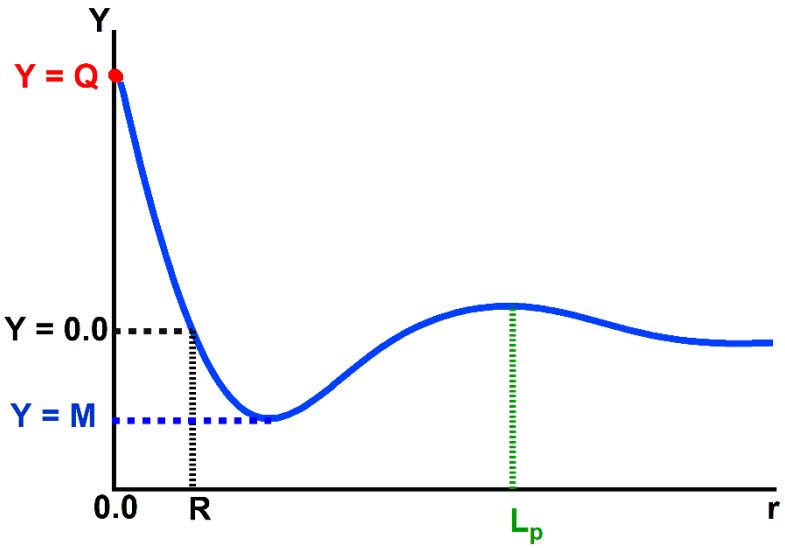


Figure 2: Example of the correlation function we obtained from SAXS measurements performed on our crystallized PEKK/PEI samples plotted as a function of the distance r. The characteristic points of the correlation function from which the lengths l_1 and l_2 involved in the lamellar stacks are determined are presented.

The correlation functions were analyzed in a conventional way [32, 33]: The invariant $Q = \int 4\pi I(q) q^2 dq$ is given by the value of the correlation function at zero. Assuming a simple two phases model where crystalline and amorphous lamellae are parallel in stacks and separated by sharp boundaries, the characteristic lengths l_1 and l_2 which correspond to the thickness of either the crystalline or interlamellar amorphous lamellae involved in the lamellar stacks were determined using the following relations:

$$Q = 2\pi(\Delta\rho)^2 \chi_1^s (1 - \chi_1^s)$$
$$M = -2\pi(\Delta\rho)^2 (\chi_1^s)^2 \qquad \text{Equation 1}$$
$$R = l_1(1 - \chi_1^s)$$
$$L_p = l_1 + l_2$$

where Δρ is the difference in electron density between crystalline and amorphous phases, $\chi_1^s, = \frac{l_1}{l_1 + l_2}$ is the volume fraction of phase 1 within the stacks and l_1 is its thickness. l_2 is the thickness of phase 2. R is the first intercept of the correlation function with the Y(r)=0. M is the value of the correlation function at its first minimum. L_p is the mean period of the stacks, determined from the first subsidiary maximum of Y(r) .

As a result, the fraction χ_1^s can be determined applying either $R/L_p = \chi_1^s(1 - \chi_1^s)$ or $\chi_1^s = \frac{-M}{-M+Q}$ and the characteristic lengths involved in lamellar stacks are given by applying the relations:

$$l_2 = \frac{R}{\chi_1^s} \; and \; L_p = \frac{l_1}{\chi_1^s} \qquad \text{Equation 2}$$

2.4. DSC analysis

Calorimetry was used to measure the crystalline fraction and characterize the glass transition of amorphous and crystallized samples. All measurements were realized with a DSC Discovery from TA Instrument that had been calibrated with indium and sapphire. The sample weights varied between 5 and 15 mg.

The entire thermal cycles undergone by amorphous and crystallized samples in the DSC setup are presented in Figure 3

A 30-min isotherm at 360°C is first applied to the sample to erase its history and obtain a fully melted sample (steps (a) and (a') in Figure 3 Then, the sample is cooled from 360°C to 60°C by applying a temperature rate of 20°C/min such that no crystallization occurs during cooling and the sample is fully amorphous at the end of the cooling (steps (b) and (b') in Figure 3). Crystallized samples are then prepared by applying an isotherm at temperature Tc to the fully amorphous samples obtained. The temperature T_c ranges between the glass transition temperature T_g and the melting temperature T_f. At the end of the crystallization isotherm, the sample is cooled from T_c to 60°C by applying a temperature rate of 20°C/min.

In this work, crystallized and fully amorphous samples are characterized under heating from 60°C to 360°C by applying a temperature rate of 10°C/min (see steps (e) and (e') in Figure 3).

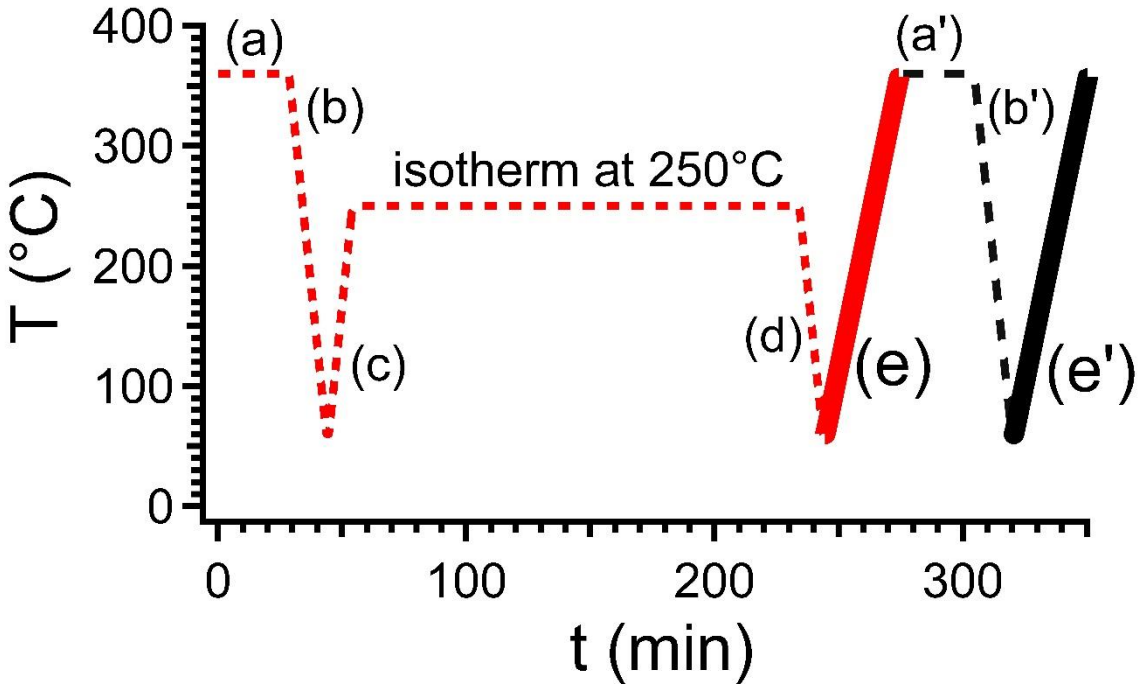


Figure 3: Thermal history applied to crystallized samples (in red) and amorphous samples (in black).

In this work, we only consider maximally crystallized samples obtained by applying a crystallization isotherm at 250°C for the duration beyond which no additional crystallization is observed. The corresponding annealing times are given in Table 1 for each blend composition.

PEKK/PEI composition	100/0	90/10	80/20	70/30	60/40	50/50
Annealing time (h)	3	2	2	2	10	15

Table 1: Annealing time at 250°C applied to prepare maximally crystallized PEKK/PEI blends

In PEKK/PEI blends, the PEKK chains are the only ones that can crystallize. As a result, the heat of fusion of 100% crystallized PEKK ΔH_f^0 is taken as the reference value to determine the crystallinity X_c of the blends. Its value is reported to be 130 J/g [34, 35].

The heat capacity is divided by the mass of the sample, and its derivative versus temperature $d\,C_p/dT$ is computed. In this work, the signal $d\,C_p^{SC}/dT$ measured on semicrystalline samples undergoing the glass transition is carefully analysed and compared to that measured on amorphous samples. We decompose $d\,C_p^{SC}/dT$ as the weighted sum of the signal of the PEKK crystal phase $d\,C_p^{C}/dT$ and that of the amorphous phases$d\,C_p^{A}/dT$.

We assume that, except in the glass transition domain, the heat capacity of the amorphous phase is not modified by the confinement between lamellae. The response of the crystal phase $d\,C_p^{C}/dT$ is thus estimated both above and below the glass transition temperature range and below the melting temperature using:

$$\frac{dC_p^C(T)}{dT} = \left(\frac{dC_p^{SC}(T)}{dT} - (1-\chi_c)\frac{dC_p^A(T)}{dT}\right)/\chi_c \qquad \text{Equation 3}$$

where χ_c is the weight fraction of the crystalline phase. Thus, it is extrapolated over the entire temperature range assuming an affine temperature dependence. The heat capacity of a crystal is known to evolve slightly nonlinearly with temperature [36], and thus, taking for its derivative an affine dependence is necessary in the present study for detailed study of the amorphous phases.

3. EXPERIMENTAL RESULTS

3.1. DSC measurements on amorphous blends

We first characterize the calorimetric response of amorphous blends. Figure 4-a presents the heat capacity as a function of temperature measured on amorphous blends at 10°C/min for various PEKK weight fractions. The curves have been shifted vertically for the sake of clarity. We emphasize that in the curves measured for the pure PEKK (100/0) and the blend PEKK/PEI 90/10 a crystallisation exotherm appears during the heating at 10°C/min. The exotherm is

followed by a melting endotherm above 250°C. The enthalpy of these two events are equal. Moreover, the two events disappear if a larger heating rate (above 20°C/min) is applied to the samples. All these features confirm that when the glass transition is measured, the samples are in their fully amorphous state. The corresponding derivative of the heat capacity with respect to temperature, i.e., dC_p/dT, is plotted as a function of temperature in Figure 4-b. The existence of a single narrow peak regardless of the composition of the mixture confirms that amorphous PEKK/PEI blends are miscible. The glass transition temperature dependence on the PEI composition follows the Fox equation, as shown in Figure 4-c.

Moreover, we observe an endotherm, which corresponds to a negative peak of dC_p/dT, immediately after the positive peak in Figure 4-b. It corresponds to physical ageing [37, 38] and will be considered in the following sections.

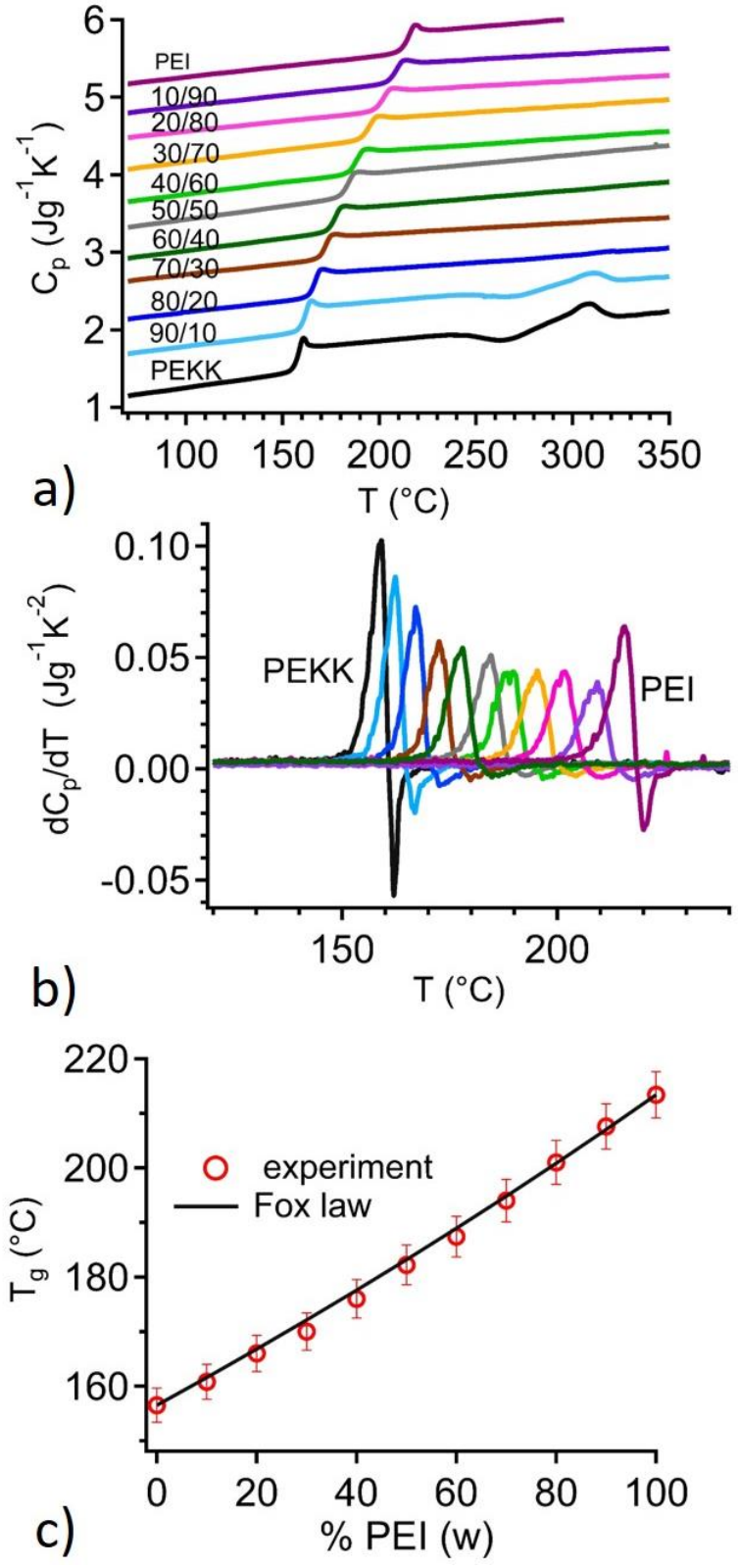


Figure 4. a) Variation in the heat capacity of PEKK/PEI amorphous blends C_p (in J g^{-1}K^{-1}) with temperature of various compositions measured by applying a heating rate of 10°C/min. b) Corresponding derivatives dC_p/dT measured during the glass transition versus temperature for

different blend compositions. c) Bulk glass transition temperature of amorphous blends as a function of the PEI weight fraction. The T_g values predicted by the Fox law are plotted as a line.

3.2. DSC measurements on crystallized samples

We will now compare the calorimetric response of maximally crystallized samples with the signal measured on the amorphous samples.

3.2.1. Pure PEKK

We first analyse the effect of crystallization on the signal measured on pure PEKK. The heat capacities of amorphous and maximally crystallized PEKK samples versus temperature (Figure 5 -a) and their derivatives (Figure 5-b) are shown in Figure 5.

The experimental data show that crystallization results in broadening of the glass transition with simultaneous disappearance of the endotherm due to the physical ageing observed in fully amorphous PEKK. Crystallization thus results in a change in the dynamics of the PEKK chains in the amorphous phases.

The melting of crystals is observed for temperatures between 260°C and 320°C. Integrating the heat flow over this temperature range gives the corresponding melting enthalpy ΔH_f. The crystal fraction is deduced by dividing ΔH_f by the reference melting enthalpy of pure PEKK crystals of large dimensions ΔH_f^0, which is equal to 130 J/g [34, 35]. We found for pure PEKK samples a maximal crystallinity of 30 wt %.

Within the precision of our measurements, we did not note any incompatibility between the crystalline fraction calculated from the melting enthalpy and the amorphous fraction obtained from the ratio of the heat capacity changes at T_g in crystallized and purely amorphous samples. As a result, we consider the so-called rigid amorphous [39, 40] fraction to be negligible in our

systems. All the amorphous fractions will be deduced from the crystalline fraction that has been calculated from the melting enthalpy.

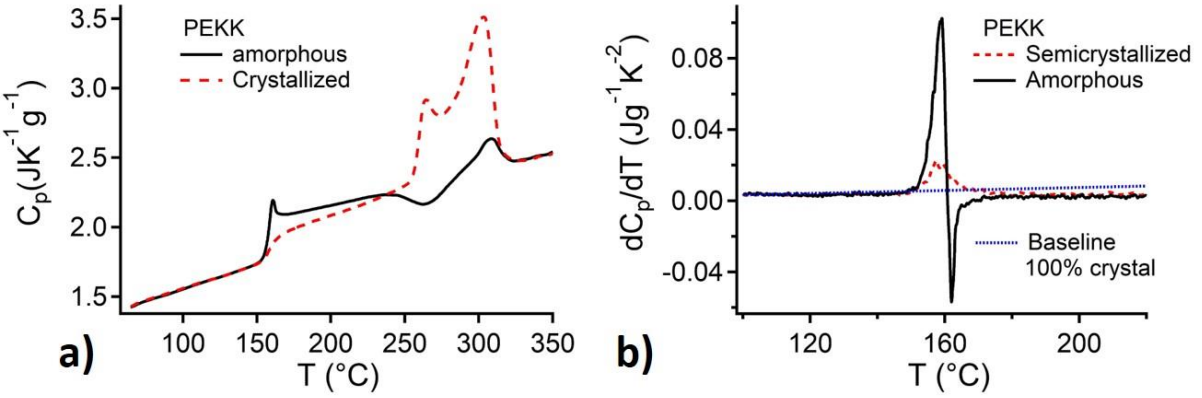


***Figure* 5.** a) Variation in the heat capacity (in J $g^{-1}K^{-1}$) of PEKK samples with temperature when applying a heating rate of 10°C/min. b) Corresponding variation in the derivative of the heat capacity dC_p/dT with respect to temperature with temperature. These curves are compared to the derivative of the heat capacity of PEKK crystals dC_p^C/dT, which we deduced by applying equation 1 (see section 2.4). The black line corresponds to signals measured on fully amorphous PEKK, while the red dotted line shows the signals measured on PEKK samples maximally crystallized at 250°C. The dotted line in blue corresponds to the deduced dC_p^C/dT.

3.2.2. PEKK/PEI blends

We now analyse the effect of a crystallization isotherm at 250°C on the calorimetric response of PEKK/PEI blends. Figure 6-a compares the temperature dependences of the heat capacity of amorphous and maximally crystallized 60/40 PEKK/PEI blends. Their corresponding derivatives with respect to temperature are presented in Figure 6-b.

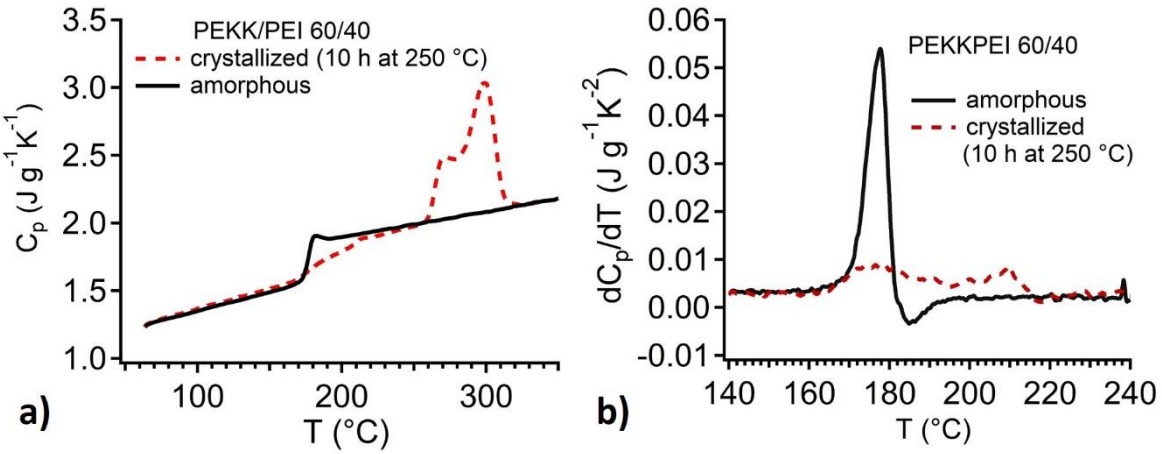


Figure **6.** a) Variation in the heat capacity (in J $g^{-1}K^{-1}$) of the PEKK/PEI blend that contains 60 wt % PEKK with temperature measured by applying a heating rate of 10°C/min. b) Corresponding variation in the derivative of the heat capacity dC_p/dT with respect to temperature with temperature. The black line corresponds to the signals measured on the fully amorphous blend, while the red dotted line shows the signals measured on the blend maximally crystallized (i.e., for 10 h) at 250°C.

Similar to pure PEKK, the glass transition domain of blends is broadened by crystallization. This feature is observed for all blend compositions. Moreover, two distinct glass transitions are observed for blends that contain more than 30 wt % PEI, revealing that the composition of the amorphous phase is no longer homogeneous in crystallized blends. Splitting of the glass transition in crystallized PEKK/PEI blends has already been observed by Dominguez et al. [24]. This suggests the coexistence of at least two different amorphous phases.

3.2.3. Crystal fraction of PEKK/PEI blends in the maximum crystallization state

We estimated the crystallinity χ_c of blend samples maximally crystallized at 250°C from the melting enthalpy. Figure 7 presents the variation in χ_c with the PEI fraction. χ_c varies nearly proportionally to the PEKK fraction, indicating that the fraction of crystalline PEKK versus the

total fraction of PEKK is constant. This means that regardless of the PEI volume fraction, the proportion of crystallized PEKK depends only on the total amount of PEKK and represents approximately 32 wt % of it. The ability to crystallize PEKK chains is the same in pure PEKK and PEKK/PEI blends. As shown in figure 8, the addition of PEI only results in a slowing down of the crystallization kinetics that can be seen with the variation of the heat flow during crystallization isotherm. The larger the PEI fraction, the later the heat flow maximum at time t_{max}. The crystallisation kinetics is driven both by the decrease of chain enthalpy due to crystallisation and the chain dynamics. For a given sample, the kinetics is maximum (i.e. t_{max} is minimum) at a given temperature that depends on the blend composition. However, the dimensions of lamellae in stacks do not change with blend composition, as we will show in part 3.3.1. Because the glass transition of the blend varies with blend composition, we plot in figure 8-b the variation of the time t_{max} as a function of the T-Tg, the temperature deviation from the glass transition temperature of the corresponding amorphous sample. We observe that the maximal crystallisation kinetics (i.e. minimum of t_{max}) is observed for a value of T-Tg that weakly depends on the PEI fraction (shift of 10K as the fraction of PEI goes from 0 to 40% w). However, the minimum value of t_{max} depends on the blend composition: its value increases by a factor 50 between the PEKK and the PEKKPEI 60/40 samples. This feature suggests a slowing down of the crystallisation kinetics as the PEI fraction increases that is larger than the one originating only from the Tg variation of the amorphous blend.

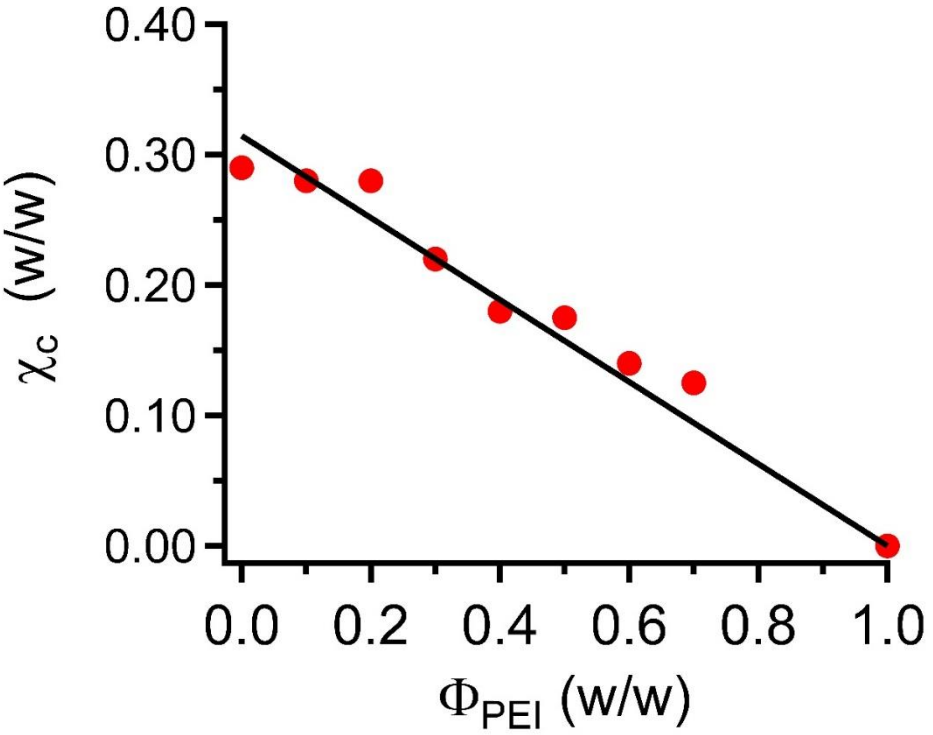


Figure 7. Crystal fraction (in weight), deduced from DSC measurements, as a function of the weight fraction of PEI for PEKK/PEI blends maximally crystallized at 250°C.

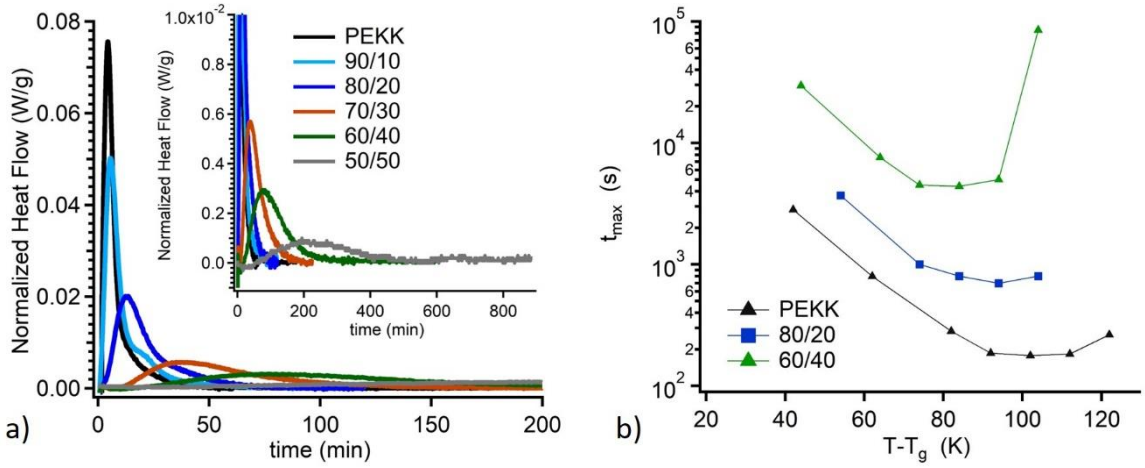


Figure 8: a) Time variation of the heat flow during the crystallisation isotherm at 250°C is plotted for various blend compositions (for the sake of clarity, an insert with a different time scale has been added). b) The time corresponding at the maximum of the heat flow variation during the isotherm is plotted as a function of the deviation of the isotherm temperature from the glass transition of the amorphous blend.

3.3. Microstructure of crystallized samples

3.3.1. SAXS measurements

The characteristic lengths of lamellar stacks were measured with SAXS. Figure 9-a presents the scattering intensity for maximally crystallized samples. The corresponding correlation function Y (r) is plotted in Figure 9-b. Applying equations 1 and 2 from the Strobl et al. method [33], we estimated the two characteristic lengths l_1 and l_2 involved in the lamellar stacks from the value of Y at the three characteristic points Q, M and R shown in figure 3.

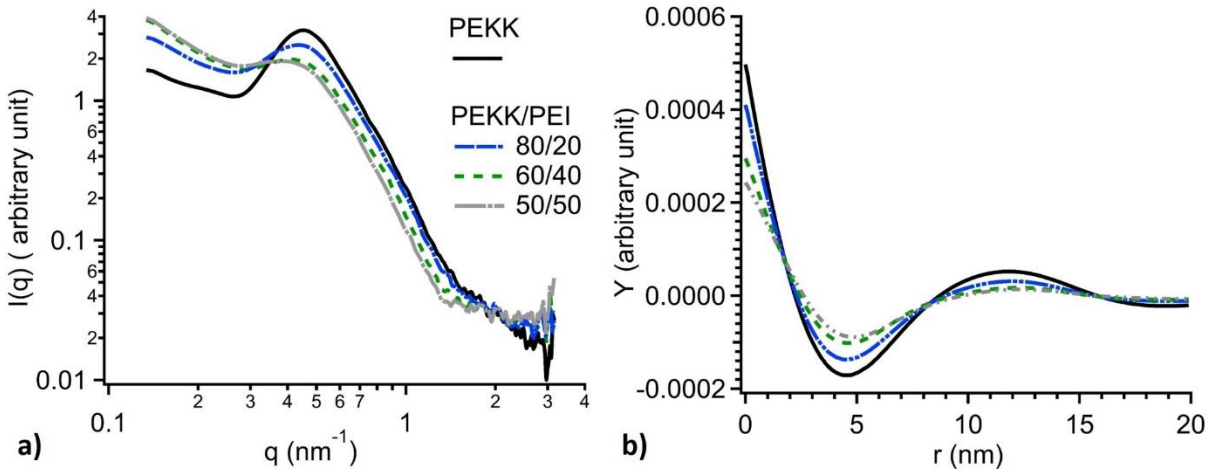


Figure 9. a) Variation in the intensity scattered by PEKK/PEI blends maximally crystallized at 250°C with the scattering vector q. b) Corresponding correlation function as a function of the distance r.

The sum of l_1 and l_2 gives the average value of the long period L_p. Notably, precise attribution of l_1 and l_2 to crystalline or amorphous lamellae, respectively, cannot be performed due to the physical principle of the SAXS measurement. We arbitrarily call l_1 the smallest characteristic length and l_2 the largest characteristic length.

The variations in l_1, l_2 and L_p with the blend composition are reported in Figure 10. Their values do not vary significantly with the PEI fraction. If there is still a slight variation, this effect is so

weak that it does not significantly modify the estimation of the interlamellar fraction. Assuming that the thicknesses of the crystalline lamellae and the amorphous interlamellar phase do not depend on the macroscopic blend composition is thus reasonable. We conclude that the amount of interlamellar amorphous phase varies in proportion to the crystalline fraction in PEKK/PEI blends maximally crystallized.

Moreover, l_1 and l_2 are found to be equal to 3.0±0.5 and 9.0±0.5 nm, respectively, resulting in a long period L_p of 12 ± 1 nm.

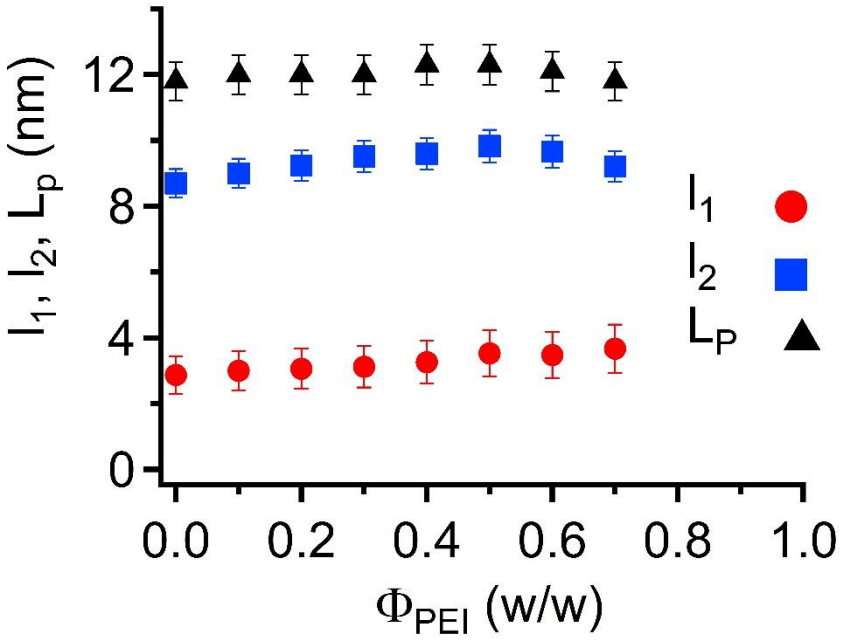


Figure 10. Variation in the characteristic lengths l_1, l_2 and L_p involved in the crystalline stacks of PEKK/PEI blends with the weight fraction of PEI, Φ_{PEI}. The data result from SAXS measurements performed on blends maximally crystallized at 250°C.

DSC measurements reveal that the crystallinity fraction of the whole sample decreases for increasing PEI fraction in blends crystallized at maximum. Moreover, the two thicknesses l_1 and l_2 involved in the lamellar stacks do not vary with blend composition. It results that the amount of crystalline phase and thus the one of the interlamellar amorphous phase in the

lamellar stacks do not depend on the PEI fraction. As a consequence, the fraction of interlamellar amorphous phase in the whole blend decreases for increasing PEI fraction, while the total amorphous fraction increases. Therefore, in addition to the interlamellar amorphous phase, there must exist amorphous domains of a different nature (interfibrillar or interspherulitic) i.e. involving length scale larger than the thickness of the interlamellar phase, which fraction increases as the PEI fraction increases.

In order to identify the nature of these amorphous phases, we performed AFM observations.

3.3.2. Microscopy observation

As previously explained, interspherulitic, interlamellar and interfibrillar amorphous phases can coexist in semicrystalline polymers. Maximally crystallized blends were observed by AFM. As shown in Figure 11, the 60/40 PEKK/PEI blend exhibits spherulites of approximately 10 μm diameter that are in contact. In order to check if there are, at the border between two spherulites, some large amorphous domains that could correspond to interspherulitic amorphous phase, we performed AFM observations at smaller scale. Figures 12-a and 12-b show typical height and phase 2*2 μm^2 images we measured for the maximally crystalized 60/40 PEKK/PEI at borders between two spherulites. The presence of anisotropic features of around 80 nm width with several orientations is observed. These elongated blocks can have different orientations. However, blocks of same orientation form domains whose dimensions are between 0.5 and 1 μm. At the border between spherulites, domains of different orientations meet.

According to these images, the border zone between spherulites does not seem to have a proper thickness. If a thickness must be attributed to the border zone, it is estimated to be less than 100 nm. These observations do not reveal any peculiar amorphous zone at the border between spherullites.

Assuming a diameter for spherulites of 10 μm and a thickness of the border zone of 100 nm, the border zones should be around 1.5% of the crystallized blend. Thus, if there is any interspherulitic phase, it is in small quantity compared to the amount of the other amorphous phases.

Therefore, we will consider that the nature of the amorphous phase is either interlamellar or interfibrillar in the PEKK/PEI blends crystalized at maximum. Thus the possible small amount of interspherulitic amorphous phase will be included in what we will call interfibrillar amorphous phase. Concerning the spatial distribution of interfibrillar phase, it is very difficult to conclude. AFM observations do not allow to directly observe the interfibrillar phase. At the borders or inside spherulites, the large domain formed by elongated blocks of 80 nm width are compactly arranged and they are not separated by large amorphous pockets.

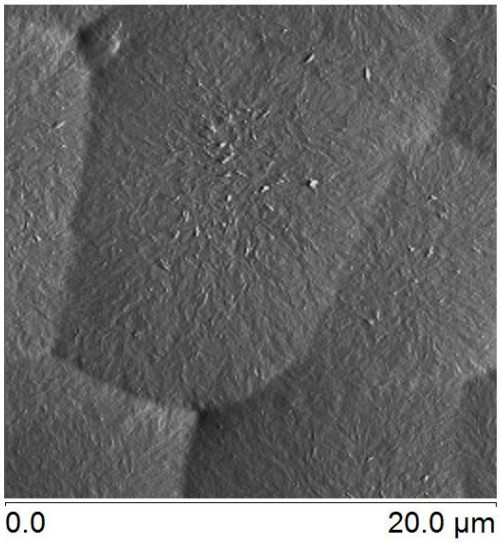


Figure 11. AFM amplitude error image of a blend with 60% PEKK and 40% PEI maximally crystallized at 250°C.

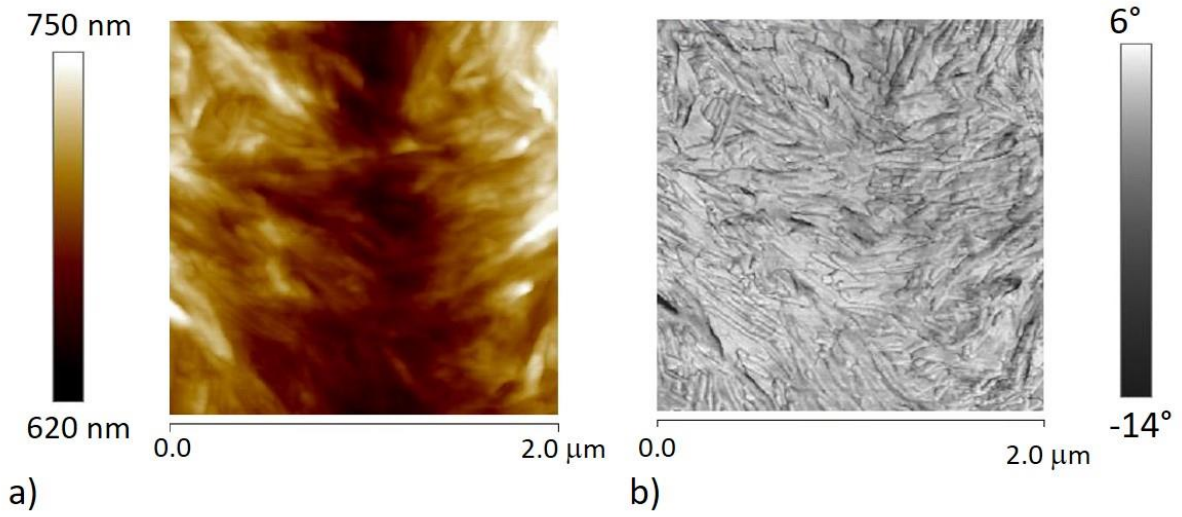


Figure 12. typical height (a) and phase (b) 2*2 μm^2 AFM images of a border between two spherulites for the PEKK/PEI 60/40 sample maximally crystallized at 250°C.

4. DISCUSSION

4.1 Different mean compositions for the interlamellar and interfibrillar phases.

According to the experimental results presented in the previous section, the amorphous chains in maximally crystallized PEKK/PEI blends are in either interlamellar or interfibrillar phases. Additionally, two distinct glass transitions are observed by calorimetry measurements once the maximally crystallized state has been reached. They result from amorphous domains with different mean compositions and different locations in the microstructure. The lowest glass transition temperature corresponds to domains rich in PEKK, while the highest T_g is related to domains rich in PEI. Moreover, the temperatures of the two glass transitions vary with the blend composition. We conclude that the two amorphous phases correspond to interlamellar and interfibrillar amorphous phases whose compositions depend on that of the macroscopic blend.

Each glass transition can now be attributed to either the interlamellar or interfibrillar amorphous phase. As explained in section 3, the amount of interlamellar amorphous phase - which is

proportional to the crystalline fraction - decreases as the PEI fraction increases, while the interfibrillar amorphous fraction simultaneously increases. Figure 13 compares the derivative of the heat capacity with respect to temperature measured on maximally crystallized blends of different macroscopic compositions. We observe that the relative weight of the first glass transition decreases while that of the second transition increases when increasing the PEI fraction. Therefore, we conclude that the lowest glass transition corresponds to the interlamellar amorphous phase and that this interlamellar phase is rich in PEKK. The highest glass transition thus corresponds to the interfibrillar amorphous phase, which is rich in PEI. We will see in the next section that the precise distribution of the composition of each phase can be deduced from calorimetry measurements. However, we first need to quantify the effect of confinement on the signals.

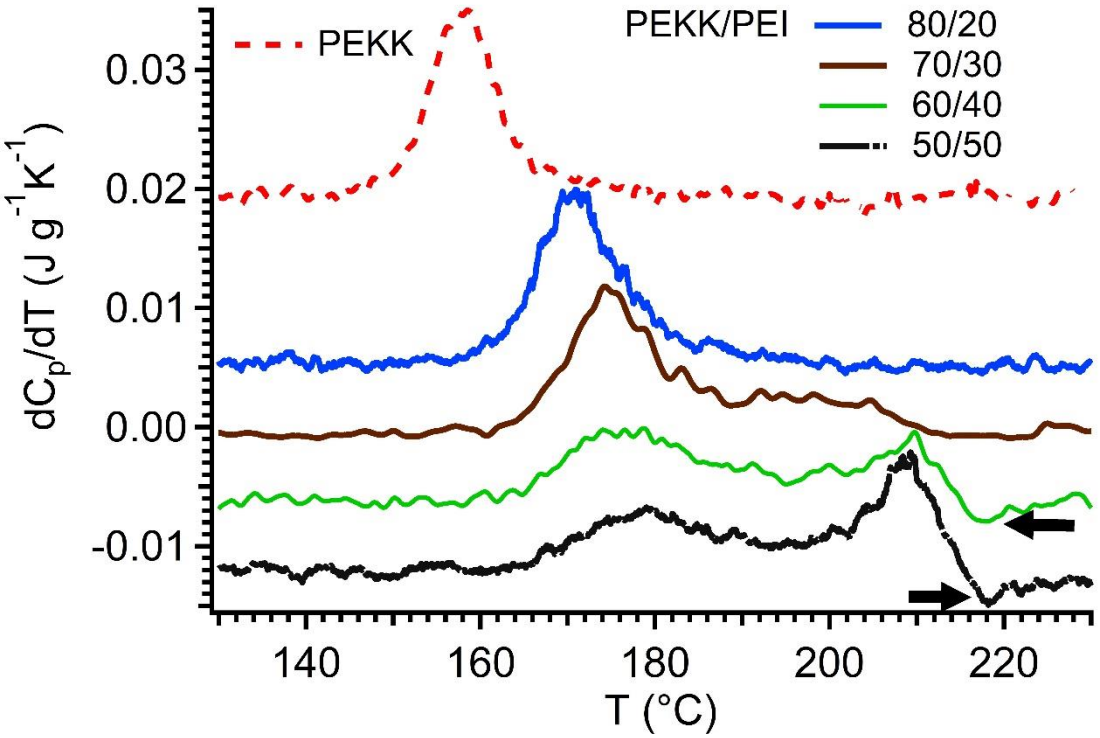


Figure 13. Temperature dependence of the derivative of the heat capacity with respect to temperature measured on PEKK/PEI blends maximally crystallized at 250°C for various PEKK/PEI blend compositions. Vertical shifts have been applied to the data for better visibility.

4.2 Confinement effects on the dynamics of amorphous PEKK chains in crystallized PEKK

According to DSC measurements, crystallization results in broadening of the glass transition domain for pure crystalline PEKK, revealing a significant modification of the dynamics of amorphous chains due to confinement between lamellae.

We will see in section 4.4 that the amount of interfibrillar phase is negligible in maximally crystallized PEKK. The amorphous chains are mainly located in interlamellar domains. The effect of confinement on the dynamics of the interlamellar amorphous phase can be estimated from the signals measured on pure PEKK. Figure 14-a compares the derivatives of the heat capacity with respect to temperature measured on fully amorphous and maximally crystallized PEKK. A rough analysis of the effect of crystallization on the width of the glass transition can be performed based on Figure 14-b. The figure compares signals that have been normalized by their maximum amplitude after subtraction of the baseline. We observe that the glass transition of amorphous chains in crystallized PEKK is widened towards both low temperatures and high temperatures.

To describe this confinement effect, we assume that confinement results in a shift in the T_g of the polymer. In this frame, the widening of the macroscopic glass transition measured for pure crystallized PEKK is equivalent to a T_g shift distribution for polymers located in the interlamellar domains. To estimate this widening effect, we assume that the signal of the confined phase can be described as the sum of the bulk signals in which the glass transition

temperature is distributed. We thus assume that the signal C_P^A of confined domains in which the glass transition is Tg is given by:

$$\frac{dC_p^A(T-T_g,T_g)}{dT} = \frac{dC_p^A(T-T_{gB},T_{gB})}{dT} \qquad \text{Equation 4}$$

where T_{gB} is the glass transition temperature of bulk amorphous PEKK and $C_p^A(T - T_{gB}, T_{gB})$ is the heat capacity at temperature T of bulk PEKK chains.

To determine the distribution of T_g in the interlamellar phase, we decompose the signal measured during the glass transition of crystallized PEKK as a sum of signals of amorphous PEKK with different glass transition temperature shifts and of the crystal signal as written in equation 5:

$$\frac{dC_p^{SC}(T)}{dT} = (1-\chi_c)\int w_C(\delta T_g)\frac{dC_p^A(T-\delta T_g)}{dT}d\delta T_g + \chi_c\frac{dC_p^C(T)}{dT}$$

$$with \int w_C(\delta T_g)d\delta T_g = 1 \qquad \text{Equation 5}$$

where $C_p^{SC}, C_p^A, \wedge C_p^C$ are the heat capacities of the semicrystalline, bulk amorphous and crystal phases, respectively; χ_c is the crystalline fraction determined from the melting enthalpy measured on the same sample; δT_g is the shift of the glass transition of confined chains with respect to that of bulk amorphous PEKK chains ($\delta T_g = T_g - T_{gB}$); and w_C is the Tg shift distribution function we want to identify.

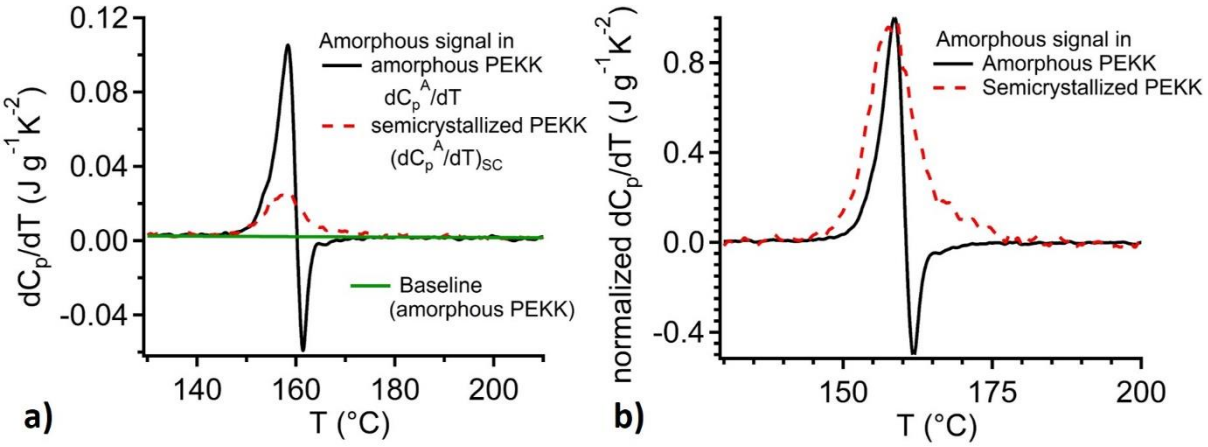


Figure 14. a) Contribution of amorphous chains to the derivative of the heat capacity with respect to temperature $\left(\frac{dC_p^A(T)}{dT}\right)_{SC}$ in maximally crystallized PEKK versus temperature. The quantity $\left(\frac{dC_p^A(T)}{dT}\right)_{SC}$ is estimated by applying equation 4 to signals measured under a temperature rate of 10°C/min. This quantity is compared to the signal measured on fully amorphous PEKK. The green line corresponds to the amorphous baseline deduced from the derivative of the heat capacity of PEKK chains in the glassy and melt states. b) Corresponding amorphous contributions normalized by their maximum value after subtraction of the amorphous baseline.

We determined the distribution function w_C by applying equation 5 in a discrete form (with a step of 0.5°C). According to the results shown in Figure 14-b, we assume both negative and positive δT_g shifts. Figure 15-a compares the experimental signal to the best description we obtained by applying the distribution w_C presented in Figure 15-b. We deduce that confinement results on average in a slowing of the dynamics for most amorphous PEKK chains. From the T_g shift distribution w_c presented in Figure 15-b, we find that the experimental mean T_g shift is approximately 8 K with a variance of approximately 100 K.

Moreover, the negative overshoot due to physical ageing observed for amorphous PEKK disappears for crystallized PEKK. This feature is also observed when the broadening of glass transition is applied to the amorphous signal [41]. So the absence of the negative overshoot due to physical ageing on the crystalized PEKK signal can be explained by the only broadening of the glass transition resulting from confinement effects.

The effect of confinement, i.e; a T_g shift and broadening can result from different mechanisms: the slowing down of the dynamics of confined chains bonded to rigid crystalline lamellae, overconcentration of chain extremities in the interlamellar phase and constraints on polymer chain segments located near the crystal interface.

We will first estimate the effect of overconcentration of chain ends on the T_g in amorphous domains in maximally crystallized PEKK. Chain extremities will likely be ejected from crystalline lamellae [42] and accumulate in the amorphous phase. In this frame, the number of chain ends per amorphous volume unit in crystallized samples is $\frac{2\rho N_a}{M(1-\chi_c)}$, where M is the molar mass of the chains, ρ is the polymer density, χ_c is the crystallinity (wt %) and N_a is Avogadro's number. The chain extremity density is thus increased by a factor of $\frac{1}{(1-\chi_c)}$ compared to that in the 100% amorphous sample. This is equivalent to a decrease in the molar mass M of the chains by a factor of $(1-\chi_c)$.

Because of the specific dynamics of chain ends, an increase in their density could result in a decrease in the glass transition temperature of amorphous chains in crystallized PEKK. To estimate this T_g shift, we apply the Fox-Flory equation that relates the glass transition temperature to the chain end density through the molar mass of chains:

$T_g(M) = T_{gB} - K/M$, where M is the molar mass of the chain and K is the Fox-Flory empirical constant that depends on the polymer nature. Thus, the T_g shift due to chain extremity overconcentration is given by:

$$\left(\delta T_g\right)_E = T_g[M.(1-\chi_c)] - T_g[M] \cong -\frac{K}{M}\left(\frac{\chi_c}{1-\chi_c}\right) \qquad \text{Equation 6}$$

We apply equation 6 to quantify the effect of overconcentration of chain ends on the Tg in amorphous domains in maximally crystallized PEKK. The value of K is not reported in the literature for PEKK chains of different molecular weights. We use the value of K reported for PEEK chains that are similar to PEKK chains. According to [43, 44, 45], K ranges between 100 kg/mol and 200 kg/mol depending on the polydispersity index of PEEK chains. Applying M=24 kg/mol, χ_c=0.3 and K = 200 kg/mol, we find a decrease in the glass transition of approximately 3 K due to overconcentration of chain ends in the amorphous phase in the maximally crystallized PEKK samples. This effect is thus small and cannot explain the observed positive shift in Tg, which is in average an increase of approximately +8 K.

Let us now consider the effect of confinement. The effect of confinement on the dynamics of amorphous polymer chains near solid surfaces, such as silica, has been the subject of abundant literature [46, 47, 48, 49, 50]. Motions of polymer segments are either hindered or accelerated near a solid interface. In the frame of dynamical heterogeneity picture,[51,52] the changes in the dynamics propagate in the direction perpendicular to the surface over a distance that depends on the strength of the interactions with the substrate. It can be approximated by a gradient of glass transition temperatures near surfaces. An expression has been proposed to describe this effect. If z is the distance from the nearest solid surface, then a positive shift of the glass transition $\delta T_g = T_{gB}\,\delta/z$ can be observed, where T_{gB} is written in absolute temperature [53] and δ is a molecular length that can be either positive or negative depending on the interactions with the substrate.

For chains in strong interaction with a solid surface, the confinement effect has been observed to result in a slowing down of the chain dynamics that depends on the distance from the solid surface [54-58]. Fryer et al.[57,58] have measured a Tg shift of 10K for PMMA thin films of 20 nm thickness in attractive interaction with a solid substrate. Dequidt et al in [59] predicted the same magnitude order for a 9nm-thick polymer film weakly interacting, with a substrate (desorption energy barrier of 0.3kT per monomer). The Tg shift of +8K we found in average for polymer chains confined in the interlamellar domains of thickness 9 nm, as we will show in the following, is in agreement with the Tg shift already observed for thin films confined between two solid substrates or in interaction with a solid substrate. In the case of polymers confined between crystalline PEKK lamellae, we observe a broadening at both low temperatures and high temperatures that is not described in literature.

Finally, the broadening could result from a third contribution related to the constraints applied by the crystal phase on the amorphous segments[60]. The chains may be pulled or twisted by their anchoring to the crystals. To our knowledge, a clear description in the literature about this effect is lacking, but we suggest that it cannot be neglected in describing the interlamellar amorphous phase dynamics.

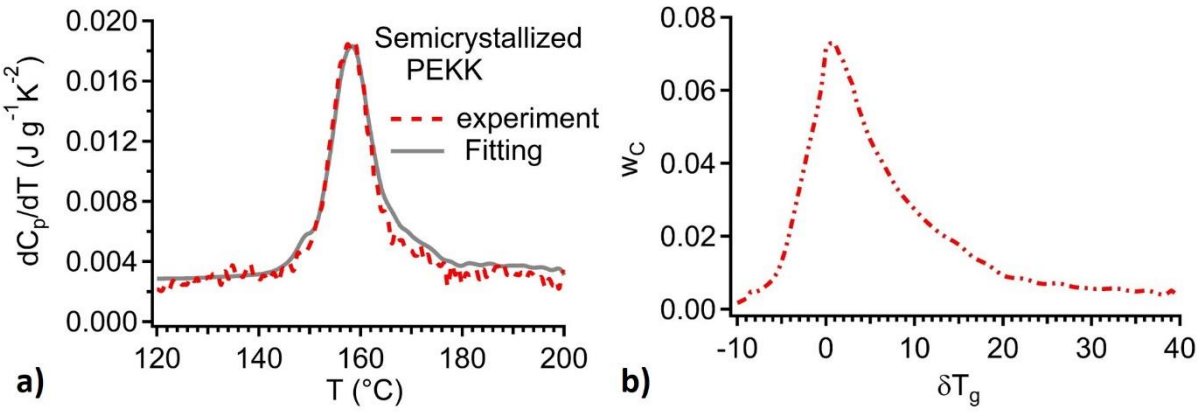


Figure 15. a) Derivative of the heat capacity with respect to temperature measured on maximally crystallized PEKK samples compared to the best description we obtained assuming

a distribution of T_g for the amorphous chains confined between crystalline lamellae. b) Distribution of the T_g shift that gives the best description of the experimental data.

4.2 Confinement of amorphous chains in crystallized blends

4.2.1 **Assumption for the confinement in interlamellar domains**

According to SAXS measurements, the characteristic lengths involved in lamellar stacking do not depend on the blend composition. Confinement effects similar to those observed in crystallized PEKK are expected in crystallized blends for polymer chains in the interlamellar amorphous phase. They would thus contribute to the broadening of the glass transition observed in crystallized blends. We will thus assume that the calorimetric response of the interlamellar amorphous PEKK/PEI blend of composition φ exhibits a widening similar to that of pure PEKK. In practice, we will write that the confined amorphous signal C_P^{AC} is just the convolution of the bulk glass transition signal with the function w_C presented in Figure 15-b according to:

$$\frac{dC_p^{AC}(T,\varphi)}{dT} = \int \frac{dC_p^{A}(T',\varphi)}{dT} w_C(T - T')\, dT' \qquad \text{Equation 7}$$

Figure 16 presents the heat capacity derivative predicted for confined 60/40 PEKK/PEI under this assumption in comparison to signals measured on bulk amorphous and maximally crystallized 60/40 PEKK/PEI blends. The broadening resulting from confinement is large; however, it does not describe the widening measured on crystallized blends alone.

We will see in the next section that this assumption on the confinement effect appears to be necessary and sufficient to describe the experimental data while respecting the constraints imposed by the macroscopic blend composition. If the effect of confinement is neglected, then coherent composition distributions for interlamellar and interfibrillar phases, agreeing with both

the data and the macroscopic blend composition constraints, cannot be found. The contribution of confinement can thus not be neglected compared to that of the composition distribution.

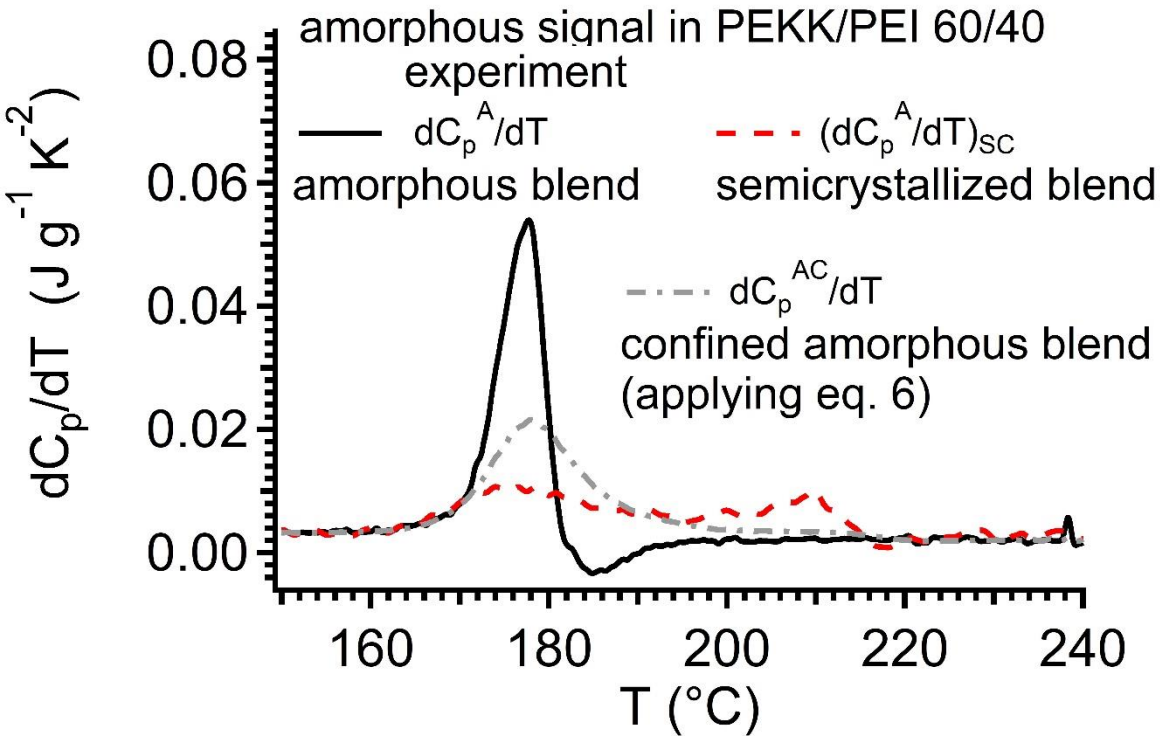


Figure 16. Heat capacity derivative $\frac{dC_p}{dT}$ measured on 60/40 PEKK/PEI blends as a function of temperature. Data measured on amorphous and crystallized blends are compared. Signals for a confined homogeneous amorphous blend are deduced by applying equation 7 and assuming the T_g shift distribution that we determined for the amorphous phase in crystallized PEKK in Figure 15.

4.2.2 **Confinement effects in the interfibrillar phase?**

Clear literature about the precise spatial distribution of the interfibrillar phase is lacking, but assuming that the effect of confinement in the interfibrillar phase, if it exists, is smaller than that observed for the interlamellar phase is reasonable. Examination of the calorimetric signal suggests that no significant effect of confinement on the dynamics of the interfibrillar phase

occurs, as we will explain now. In section 4.1, we showed that the interfibrillar phase is rich in PEI with a glass transition that occurs in the highest temperature range.

In the previous sections, we have shown that confinement effects broaden the glass transition, resulting in the disappearance of the macroscopic negative overshoot observed for aged bulk amorphous polymers. However, in Figure 13, a weak negative overshoot – see the arrow in Figure 13 – is obvious at high temperatures for crystallized blends with a PEI fraction higher than 30%. Its amplitude increases when applying, after the crystallization isotherm - i.e., for steps (d) and (e) in Figure 3 - a slower temperature rate, as shown Figure 17-a, which compares the signals measured on 50/50 PEKK/PEI blends when applying temperature rates of 20°C/min and 3°C/min.

A similar trend is observed for pure PEI samples subject to a slower temperature rate from the melt state, i.e., for steps (b') and (e') in Figure 3, as shown in Figure 17-b. However, such a macroscopic ageing endotherm is not observed in the case of crystallized PEKK if slower temperature rates are applied after the crystallization isotherm (see Figure 17-a).

Therefore, the macroscopic signature of physical ageing is not the same for confined and nonconfined amorphous phases aged under the same conditions. Confinement results in broadening of the glass transition, described by a T_g shift distribution leading to the disappearance of the macroscopic ageing endotherm in confined amorphous phases compared to bulk amorphous samples that undergo the same physical ageing. The results measured on crystallized PEKK (see Figure 17-a) confirm that no endotherm is observed even for the lowest temperature rate applied. This is not the case for the right glass transition peak of the crystallized blends. Therefore, the observation of the ageing endotherm at the right wing of the second glass transition in crystallized PEKK/PEI blends suggests that the effect of confinement – if it exists – is not significant for the interfibrillar phase.

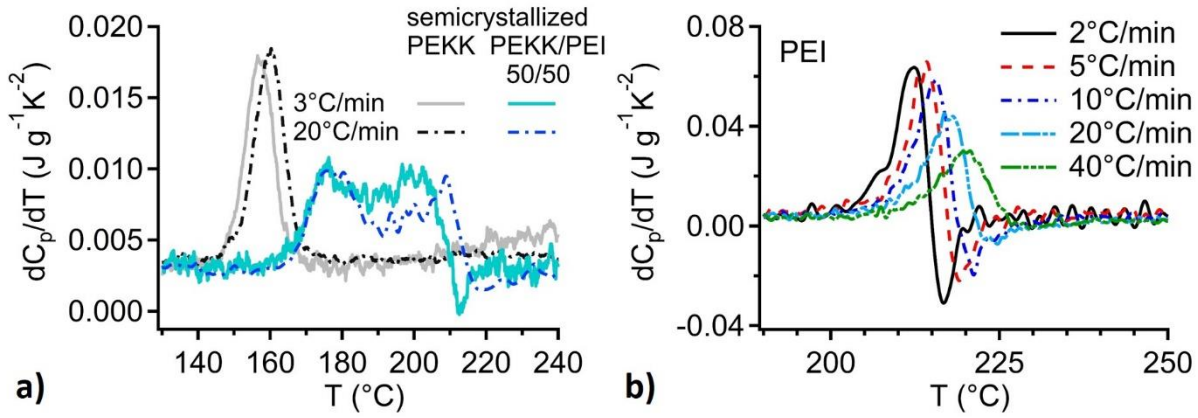


Figure 17. a) Effect of the temperature rate on the shape of heat capacity derivative $\frac{dC_p}{dT}$ for pure PEKK and 50/50 PEKK/PEI. Measurements were performed by applying temperature rates of 20°C/min or 3°C/min for steps (d) and (e) in Figure 3. b) Evolution of the shape of the heat capacity derivative $\frac{dC_p}{dT}$ measured on pure PEI as a function of the temperature rate $\frac{dT}{dt}$. Measurements were performed by applying $\frac{dT}{dt}$ values ranging between 2°C/min and 40°C/min for steps (b') and (e') of the thermal cycle (see Figure 3).

All these experimental observations lead to the following conclusion: in PEKK/PEI crystallized blends with PEI fractions ranging between 30% and 60%, two amorphous phases with different compositions coexist. Since the polymers PEKK and PEI are miscible in all proportions in the amorphous state, these two phases must belong to different environments, which must correspond to interlamellar and interfibrillar amorphous phases. The high temperature glass transition corresponds to unconfined polymer chains that should be in the interfibrillar amorphous phase. Therefore, the low temperature glass transition corresponds to the interlamellar amorphous phase. As a result, crystallized PEKK/PEI blends consist of three main phases: a crystalline phase with only PEKK, an interlamellar amorphous phase rich in PEKK that undergoes a confinement effect, and an interfibrillar amorphous phase rich in PEI that does

not undergo any significant confinement effect. We can now turn to the precise determination of the PEKK/PEI distribution in each of the amorphous phases.

4.3 Composition distribution in amorphous phases in crystallized blends

In the previous section, we showed that the broadening of the calorimetric signal due to confinement is small compared to the observed broadening in blends (see Figure 16). Moreover, the width of the low temperature glass transition related to the interlamellar phase is larger than that of a confined homogeneous blend of the same average composition. The same observation can be made for the high temperature glass transition measured on the crystallized blends. Thus, a composition distribution must be involved to discuss the calorimetric response shown in Figure 16.

The composition distributions of the two amorphous phases are quantitatively determined from the analysis of the derivative of the heat capacity with respect to temperature measured on crystallized blends. The DSC response of crystallized blends is given by the sum of the responses of all phases weighted by the fraction of each phase in the material. In addition to the crystalline phase, we identified two amorphous phases that differ by their average composition and average confinement degree.

As explained in the previous sections, the response of the interfibrillar phase exhibits no confinement effects and is thus only driven by the composition distribution. Locally, the interfibrillar amorphous phase can be described as a distribution of nonconfined amorphous domains differing by their PEI fraction φ . The DSC response of the interfibrillar amorphous phase is thus the integral of the signal of the bulk amorphous sample $\frac{dC_p^A(T,\varphi)}{dT}$ shown in Figure 4-b - weighted by a composition distribution function that we call $\alpha_B(\varphi)$.

In contrast, the response of the interlamellar phase results from both the composition distribution and confinement. Its calorimetric signal is thus the integral of signals of confined blends of composition φ weighted by a composition distribution function $\alpha_C(\varphi)$. As explained above, we assume that the signal of a confined blend -$\frac{dC_p^{AC}(T,\varphi)}{dT}$ - is equal to the convolution of that of a homogenous blend of composition φ in its amorphous state with the function w_C (see equation 7).

Moreover, for blends with PEI fractions ranging between 30% and 60%, the glass transition measured on maximally crystallized samples is split into two distinct well-separated parts that we attribute exclusively to either the interlamellar phase (the low temperature part) or interfibrillar phase (high temperature part).

In doing so, we assume a PEI composition for domains in the interlamellar phase less than a threshold composition φ_S. The PEI composition for domains in the interfibrillar phase is greater than φ_S. The threshold PEI composition is chosen such that the temperature at the minimum of the signal corresponds to the glass transition temperature of a homogenous amorphous blend of composition φ_S.

In this frame, the response measured on a crystallized blend is given by the relation:

$$\frac{dC_p^{SC}(T)}{dT} = (1-\chi_c)\left(\int_{\varphi=0}^{\varphi=\varphi_s} \alpha_C(\varphi)\frac{dC_p^{AC}(T,\varphi)}{dT}d\varphi + \int_{\varphi=\varphi_s}^{\varphi=1} \alpha_B(\varphi)\frac{dC_p^{A}(T,\varphi)}{dT}d\varphi\right) + \chi_c \frac{dC_p^{C}(T)}{dT}$$ where

$$\frac{dC_p^{AC}(T,\varphi)}{dT} = \int \frac{dC_p^{A}(T\prime,\varphi)}{dT} w_C(T-T')\,dT' \qquad \text{Equation 8}$$

The composition distribution $\alpha=\alpha_c+\alpha_B$ has to meet two constraints: first, the mass conservation of matter. Second, the global composition has to correspond to that of the sample, which is known. The two constraints are described by the following equations:

$$\int_0^{\varphi_s} \alpha_C(\varphi)d\varphi + \int_{\varphi_s}^1 \alpha_B(\varphi)d\varphi = 1 \qquad \text{Equation 9}$$

$$\int_0^{\varphi_s} \varphi.\alpha_C(\varphi)d\varphi + \int_{\varphi_s}^1 \varphi.\alpha_B(\varphi)d\varphi = \Phi_{PEI}/(1-\chi_c) \qquad \text{Equation 10}$$

We now have to identify the composition distribution α that eventually gives a good description of the experimental data. We restrict our analysis to blend compositions ranging between 30% and 50%, for which splitting of the glass transition is clearly observed. Only the first constraint is applied, and the second constraint is checked afterwards.

In Figure 18-a, data measured on a blend with 60% PEKK and 40% PEI crystallized at 250°C for 10 h are compared to the best fit obtained by applying equations 8 and 9 and φ_S=0.7. The corresponding distribution of the PEI composition is presented in Figure 18-b and results in a total PEKK fraction of 60 wt %, in agreement with the macroscopic composition of the blend. A good description was also obtained for maximally crystallized blends containing 30 wt % and 50 wt % PEI (see Figure 18). Note also that the confinement effect has to be taken into account to obtain a proper result. This confirms the hypotheses of our description:

- the low glass transition temperature phase is the interlamellar phase, for which the confinement effects must be taken into account,

- the high glass transition temperature phase is the interfibrillar phase, which exhibits no confinement effect, and

- both phases exhibit a significant concentration distribution.

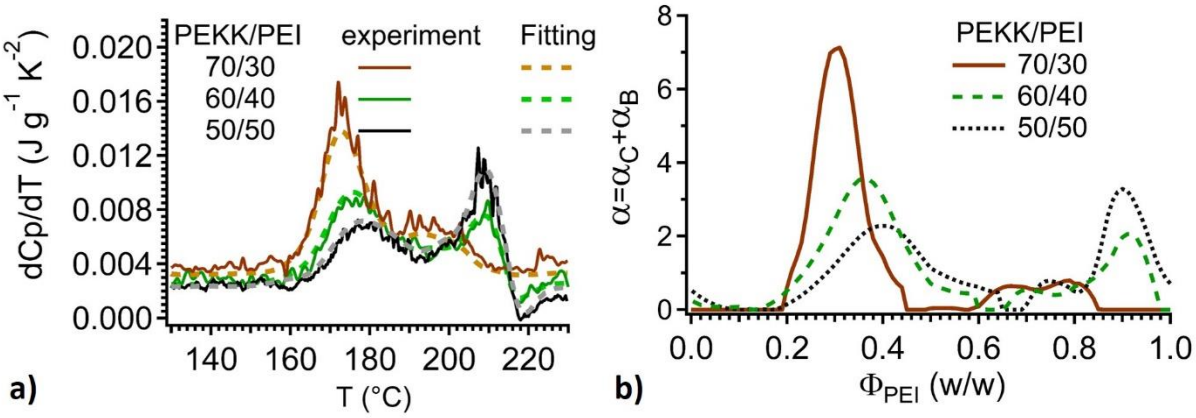


Figure 18. a) Derivative of the normalized heat capacity measured on PEKK/PEI blends maximally crystallized at 250°C (solid lines) and the fit (dashed lines) identified by applying equations 8 and 9. The PEI composition threshold between confined and bulk signals φs was taken to be 0.45 for the 30 wt % PEKK/PEI blend (70/30), 0.7 for the 40 wt % PEKK/PEI blend (60/40) and 0.65 for the 50 wt % PEKK/PEI blend (50/50). b) Corresponding composition distribution as a function of the PEI fraction.

The fractions of interlamellar and interfibrillar phases can be estimated from the identified composition distribution of the two amorphous phases, leading to the attribution of the thicknesses l_1 and l_2 involved in the lamellar stacks.

The crystalline volume fraction in the stacks χ_c^s, which corresponds to the crystalline fraction measured by SAXS, is given by:

$$\chi_c^s = \frac{\chi_c}{\chi_c + \frac{\rho_c}{\rho_A}\chi_{IL}} \qquad \text{Equation 11}$$

where ρ_c and ρ_a are the densities of the crystalline and amorphous phases, respectively, χ_c is the weight fraction of the crystalline phase and χ_{IL} is the weight fraction of the interlamellar amorphous phase, which is given by:

$$\chi_{IL} = (1 - \chi_c)\int_0^{\varphi_s} \alpha_C(\varphi)d\varphi \qquad \text{Equation 12}$$

The quantity χ_c^s should be equal to the ratio between the thickness of the crystalline lamellae and the long period ($\chi_c^s = l_c/L_p$, where l_c is either l_1 or l_2, as discussed in section 3.3.1).

For a blend composed of 60% PEKK maximally crystallized after 10 h at 250°C, we find χ_c=0.22 and $\chi_{IL} = 0.58$. Therefore, $\chi_c^s = 0.26$ using ρ_a=1.27 g/cm^3 and ρ_c=1.4 g/cm^3.

We can identify that l_c corresponds to l_1, i.e., to 3 nm, and thus, the average thickness of the amorphous layer is 9 nm. Using this, we also verify that in maximally crystallized PEKK, the interfibrillar fraction is negligible, as hypothesized in section 4.2.

Therefore, our analysis reveals the following characteristics of the morphology. The PEI weight fraction in the interfibrillar phase is significantly higher than that in the interlamellar phase for samples with more than 30% PEI. For samples with PEI initial volume fractions below 50%, the composition of the interlamellar phase is on the same order as the initial volume fraction.

4.5 Origin of the arrangement of the amorphous phase

According to the results presented in the previous sections, the interlamellar and interfibrillar amorphous phases do not have a single composition over the sample, and the compositions of both phases are distributed. We suggest the following mechanisms to explain these two distributions.

During crystallization, the PEI chains are partly excluded from the interlamellar phase. As a consequence, the PEI fraction of the amorphous phase at the growth front probably increases during the advance of the crystallization front. As a result, the PEI fraction in the interlamellar amorphous phase confined at the beginning of crystallization might be lower than that in the phase confined at the end. For the same reason, the composition of the interfibrillar phase should become increasingly richer in PEI during the advance of the crystallization front. The

scale at which this phenomenon occurs is unclear, but AFM images from Debier et al. [3] suggest that this mechanism occurs at the scale of dendrites. One can also wonder whether these two phases can become homogeneous under annealing. We did not observe such a phenomenon: the width of the distribution appears to not evolve with time under annealing of at least 5 h once maximum crystallization has been reached. The topology of the crystalline structure is so complex that equilibration of the interfibrillar phase by diffusion is either impossible or at least extremely slow.

Additionally, the thicknesses of lamellar stacks and amorphous interlamellar layers may be distributed. The correlation peak measured by SAXS is in fact quite broad, suggesting a distribution of the characteristic thicknesses of lamellar stacks. Because confinement excludes PEI from the interlamellar phase, the disorder of the interlamellar thickness may lead to a composition distribution of the interlamellar phases.

5. CONCLUSION

In semicrystalline/amorphous blends of miscible polymers, the amorphous polymer is expelled from the crystalline lamellae. In PEKK/PEI systems, this results in a splitting of the amorphous phase into interlamellar and interfibrillar phases with distinct average compositions. Introducing a new calorimetric analysis of the glass transition of semicrystalline polymers, we quantitatively estimate the effects of both confinement and the composition distribution on the dynamics of the amorphous phases in semicrystalline PEKK/PEI blends. For this, we decompose the temperature derivative of the calorimetric signal into signals of amorphous blends with various compositions, taking into account the effect of confinement. We show that the confinement effect occurs only in the interlamellar phase. We observe that the confinement results on average in a slowing down of the dynamics. However, it also results in a broadening

of the glass transition towards lower temperature, i.e., a small but nonnegligible portion of chains undergo acceleration of their dynamics. We also show that the interfibrillar phase is very concentrated in PEI, while the interlamellar phase contains a small fraction of PEI. This suggests the following mechanism: During crystallization, PEI chains are partly excluded from the interlamellar phase and thus accumulate in the interfibrillar phase.

REFERENCES

1 Hubert, L.; David, L.; Seguela, R.; Vigier, G.; Degoulet, C.; Germain, Y. Physical and mechanical properties of polyethylene for pipes in relation to molecular architecture. I. Microstructure and crystallisation kinetics. *Polymer* **2001**, 42, 8425-8434

2 Agari, Y. ; Ueda, A. ; Omura, Y. ; Nagai, S. Thermal diffusivity and conductivity of PMMA/PC blends. *Polymer* **1997**, 38, 801–807. https://doi.org/10.1016/S0032-3861(96)00577-0

3 Debier, D.; Jonas, A.M.; Legras, R. Blends of polycarbonate and acrylic polymers: Crystallization of polycarbonate. *J. Polym. Sci., Part B: Polym. Phys* **1998**, 36, 2197–2210.

4 Lu, B., Lamnawar, K., Maazouz, A., Zhang, H., 2016. Revealing the dynamic heterogeneity of PMMA/PVDF blends: from microscopic dynamics to macroscopic properties. *Soft Matter*, **2016**, 12, 3252–3264. https://doi.org/10.1039/C5SM02659H

5 Aid, S.; Eddhahak, A.; Khelladi, S.; Ortega, Z.; Chaabani, S.; Tcharkhtchi, A.; On the mis-cibility of PVDF/PMMA polymer blends: Thermodynamics, experimental and numerical investi-gations. *Polymer Testing* **2019**, 73, 222-231. https://doi.org/1016/j.polymertesting.2018.11.036

6 Korskanov, V; Fesenko, O Miscibility of Poly(Methyl Methacrylate) and Poly(Vinylidene Fluoride) Examined by Thermally Stimulated Depolarization Current and Dielectric

Relaxation Spectroscopy. *J. Macromol. Science. Part B Physics*, 10.1080/00222348.2020.1847393

7 Koseki, Y.; Aimi, K.; Ando, S. Crystalline structure and molecular mobility of PVDF chains in PVDF/PMMA blend films analyzed by solid-state F-19 MAS NMR spectroscopy. *Polymer Journal* **2012**, 44)8 ,(757-763.

8 Oikonomou, EK..; Tence-Girault, S.; Gerard, P.; Norvez, S. Swelling of semi-crystalline PVDF by a PMMA-based nanostructured diblock copolymer: Morphology and mechanical properties. *Polymer* **2015**, 76 , 89-97 DOI: 10.1016/j.polymer.2015.08.055

9 Russell, T. P.; Ito, H.; Wignall, G. D. Neutron and x-ray scattering studies on semicrystalline polymer blends. *Macromolecules* **1988**, 21, 1703–1709. https://doi.org/10.1021/ma00184a029

10 Jin, X.; Zhang, S.; Runt, J. Broadband Dielectric Investigation of Amorphous Poly(methyl methacrylate)/Poly(ethylene oxide) Blends. *Macromolecules* **2004**, 37, 8110–8115. https://doi.org/10.1021/ma049281b

11 E. Martuscelli, in Polymer Blends: Processing, Morphology and Properties E. Martuscelli, R. Palumbo, and M. Kryszewski (eds.), pp 23-47, Plenum Press, NewYork, **1979**

12 Angialosi, D.; Alegría, A.; Colmenero, J. Cooling Rate Dependent Glass Transition in Thin Polymer Films and in Bulk. In Fast Scanning Calorimetry; Springer: Cham, **2016**; pp 403−431

13 Hudson, S. D.; Davis, D. D.; Lovinger, A. J. Semicrystalline morphology of poly(aryl ether ether ketone)/poly(ether imide) blends. *Macromolecules* **1992**, 25, 1759–1765. https://doi.org/10.1021/ma00032a021

14 Nguyen, T. L.; Bédoui, F.; Mazeran, P.-E.; Guigon, M. Mechanical Investigation of Confined Amorphous Phase in Semicrystalline Polymers: Case of PET and PLA. *Polym. Eng. Sci.* **2015**, 55 (2), 397–405. https://doi.org/10.1002/pen.23896.

15 Simon, F. T. ; Rutherford Jr., J. M.; Crystallization and melting behavior of polyethylene oxide copolymers. *J. Appl. Phys.* 1964, 35, 82- https://doi.org/10.1063/1.1713103

16 Fragiadakis, D., Runt, J.,; Microstructure and Dynamics of Semicrystalline Poly(ethylene oxide)−Poly(vinyl acetate) Blends. *Macromolecules* **2010**, 43, 1028–1034. https://doi.org/10.1021/ma9020938

17 Huo, P.P., Cebe, P., Capel, M.; Dynamic mechanical relaxation and x-ray scattering study of poly(butylene terephthalate)/polyarylate blends. *Macromolecule*s **1993**, 26, 4275–4282. https://doi.org/10.1021/ma00068a031

18 Jonas, A. M.; Ivanov, D.A.; Yoon, D. Y. The Semicrystalline Morphology of Poly(ether−ether−ketone) Blends with Poly(ether−imide). *Macromolecules* **1998**, 31, 5352–5362. https://doi.org/10.1021/ma9711607

19 Talibuddin, S., Wu, L., Runt, J., Lin, J.S., 1996. Microstructure of Melt-Miscible, Semicrystalline Polymer Blends. *Macromolecules* **1996**, 29, 23, 7527–7535 https://doi.org/10.1021/ma960508f

20 Hudson, S.D., Davis, D.D., Lovinger, A.J., Semicrystalline morphology of poly(aryl ether ether ketone)/poly(ether imide) blends. *Macromolecules* **1992,** 25, 1759–1765. https://doi.org/10.1021/ma00032a021

21 Hsiao, B. S. ; Sauer B., B. Glass transition , Crystallization and morphology relationships in miscible Poly(Aryl Ether ketones) and Poly(ether imide) blends, *J. Polym. Sci. B Polym. Phys.***1993,** 31, 901

22 Keith, H. D.; Padden, F. J. Spherulitic Crystallization from the Melt. I. Fractionation and Impurity Segregation and Their Influence on Crystalline Morphology. *J. Appl. Phys.* **1964**, 35 (4), 1270–1285. https://doi.org/10.1063/1.1713606.

23 Keith, H.D.; Padden, F.J. Influence of reptation on localized diffusion in crystallizing polymers. *J. Polym. Sci. B Polym. Phys.* **1987**, 25, 230–242. https://doi.org/10.1002/polb.1987.090250117

24 Dominguez, S., Derail, C., Léonardi, F., Pascal, J., Brulé, B., Study of the thermal properties of miscible blends between poly(ether ketone ketone) (PEKK) and polyimide. *Eur. Polym. J.* **2015**, 62, 179–185. https://doi.org/10.1016/j.eurpolymj.2014.10.024

25 Sabic Technical data Ultem Resin at https://www.sabic.com/en/products/specialties/ultem-resins/ultem-resin

26 D. Bashford, Thermoplastics, Chapman & Hall, 1997

27 Choupin Tanguy Mechanical performances of PEKK thermoplastic composites linked to their processing parameters. Mécanique des matériaux [physics.class-ph]. Ecole nationale supérieure d'arts et métiers - ENSAM, 2017. Français.

28 Technical data 6000 series Arkema Inc at https://www.arkema.com/export/shared/.content/media/downloads/products-documentations/incubator/arkema-kepstan-6000-tds.pdf

29 Li, C.; Strachan, A. Prediction of PEKK properties related to crystallization by molecular dynamics simulations with a united-atom model. *Polymer* **2019**, 174, 25-32, https://doi.org/10.1016/j.polymer.2019.04.053.

30 Blundell, D. J.; Newton, A. B. Variations in the crystal lattice of PEEK and related para-substituted aromatic polymers: 2. Effect of sequence and proportion of ether and ketone links. *Polymer* **1991**, 32(2), 308-313, https://doi.org/10.1016/0032-3861(91)90019-F.

31 Kendrick, J. ; Robson, E. ; Weaver, M. Ab initio and Molecular Mechanics Study of Polyaryl Ether Ketone Polymers. *J. Chem. Soc. FARADAY TRANS*. **1995**, 91(16), 2609-2614

32 Rabiej, S.; Rabiej, M. Determination of the parameters of lamellar structure of semicrystalline polymers using a computer program SAXSDAT. *Polimery* **2011**, 56, 662–670. https://doi.org/10.14314/polimery.2011.662

33 Strobl, G. R.; Schneider, M. Direct evaluation of the electron density correlation function of partially crystalline polymers. *J. Polym. Sci. B Polym. Phys.* **1980**, 18, 1343–1359. https://doi.org/10.1002/pol.1980.180180614

34 Chang, I. Y.; Hsiao, B. S. Thermal properties of high performance thermoplastic composites based on poly (ether ketone ketone)(PEKK), in: International SAMPE Symposium and Exhibition, 36 Th, San Diego, CA. **1991**, 1587–1601.

35 Quiroga Cortes, L. ; Lonjon, A.; Dantras, E.; Lacabanne, C. High-performance thermoplastic composites poly(ether ketone ketone)/silver nanowires: Morphological, mechanical and electrical properties. *J. Non-Cryst. Solids* **2014**, 391, 106-111. https://doi.org/10.1016/j.jnoncrysol.2014.03.016

36 Wunderlich B. The ATHAS database on heat capacities of polymers. *Pure & App. Chem*. **1945**, 67(6), 1019-1026.

37 Echeverria, I. ; Su, P.- C.; Simon, S.; Plazek, D.J. Physical Aging of a Polyetherimide: Creep and DSC Measurements. *J. Polym. Sci. B Polym. Phys*. **1995**, 33, 2457-2468

38 Struik L. C. E., Physical aging in amorphous polymers and other materials, Elsevier Amsterdam, **1978**. pp. 229.

39 Mathot V. B. F. Calorimetry and thermal analysis of polymers, V.B.E Mathot (Ed.), Hanser, Munich, **1994,** pp 377.

40 Struik, L. C. E., The mechanical behaviour and physical ageing of semicrystalline polymers: 2. *Polymer* **1987**, 28(9), 1534-1542.

41 Papon, A.; Montes, H.; Hanafi, M.; Lequeux, F.; Guy, L.; Saalwachter, K. Glass-Transition Temperature Gradient in Nano-¨composites: Evidence from Nuclear Magnetic Resonance and Differential Scanning Calorimetry. *Phys. Rev. Lett.* **2012**, 108, 065702

42 Aharoni, S. M.; Harget, P. J. On the location of chain-ends in rapidly crystallized poly(ethylene terephthalate). *J. Polym. Sci. B Polym. Phys*. **1978**, 16, 159-169. doi:10.1002/pol.1978.180160114

43 M. Day, Y. Deslandes, J. Rooverst and T. Suprunchuk Effect of molecular weight on the crystallization behaviour of poly(aryl ether ether ketone): a differential scanning calorimetry study. *Polymer*, **1991**, 32(7) 1258-1266

44 Fougnies, C.; Dosiere, M.; Koch, M. H. J.; Roovers, J. Cold Crystallization of Narrow Molecular Weight Fractions of PEEK. *Macromolecules* **1999**, 32(24), 8133-8138

45 Courvoisier, E. ; Bicaba, Y. ; Xavier Colin, X. Analyse de la dégradation thermique du Poly(éther éther cétone) Matériaux & Techniques, 2017, 105, 403

46 Cheng, S.; Carroll, B.; Lu, W.; Fan, F.; Carrillo, J.-M. Y.; Martin, H.; Holt, A. P.; Kang, N.-G.; Bocharova, V.; Mays, J. W.; Sumpter, B. G.; Dadmun, M.; Sokolov, A. P. Interfacial Properties of Polymer Nanocomposites: Role of Chain Rigidity and Dynamic Heterogeneity Length Scale. *Macromolecules* **2017**, 50 (6), 2397–2406. https://doi.org/10.1021/acs.macromol.6b02816.

47 Klüppel, M. Evaluation of Viscoelastic Master Curves of Filled Elastomers and Applications to Fracture Mechanics. *J. Phys. Condens. Matter* **2009**, 21 (3), 035104. https://doi.org/10.1088/0953-8984/21/3/035104.

48 Mujtaba, A.; Keller, M.; Ilisch, S.; Radusch, H.-J.; Beiner, M.; Thurn-Albrecht, T.; Saalwächter, K. Detection of Surface-Immobilized Components and Their Role in Viscoelastic Reinforcement of Rubber–Silica Nanocomposites. *ACS Macro Lett.* **2014**, 3 (5), 481–485. https://doi.org/10.1021/mz500192r.

49 Nguyen, H. K.; Liang, X.; Ito, M.; Nakajima, K. Direct Mapping of Nanoscale Viscoelastic Dynamics at Nanofiller/Polymer Interfaces. *Macromolecules* **2018**, 51 (15), 6085–6091. https://doi.org/10.1021/acs.macromol.8b01185.

50 Papakonstantopoulos, G. J.; Doxastakis, M.; Nealey, P. F.; Barrat, J.-L.; de Pablo, J. J. Calculation of Local Mechanical Properties of Filled Polymers. *Phys. Rev. E* **2007**, 75 (3), 031803. https://doi.org/10.1103/PhysRevE.75.031803.

51 Merabia, S., Long, D. Heterogeneous dynamics at the glass transition in van der Waals liquids: Determination of the characteristic scale. *Eur. Phys. J. E* **9,** 195–206 (2002). https://doi.org/10.1140/epje/i2002-10084-2

52 Masurel, R. J. ; Gelineau, P. ; Cantournet, S. ; Dequidt, A. ; Long, D. R. ; Lequeux, F. ; Montes, H., Role of Dynamical Heterogeneities on the Mechanical Response of Confined Polymer, *Phys. Rev. Lett.* **2017**, 118, 047801

53 Long, D.; Lequeux, F. Heterogeneous dynamics at the glass transition in van der Waals liquids, in the bulk and in thin films. *Eur. Phys. J. E: Soft Matter Biol. Phys.* **2001**, 4, 371−387.

54 Batistakis, C.; Michels, M. A. J.; Lyulin, A. V. Confinement-Induced Stiffening of Thin Elastomer Films: Linear and Nonlinear Mechanics vs Local Dynamics. Macromolecules **2014**, 47 (14), 4690–4703. https://doi.org/10.1021/ma5003744.

55 Nguyen, H. K.; Sugimoto, S.; Konomi, A.; Inutsuka, M.; Kawaguchi, D.; Tanaka, K. Dynamics Gradient of Polymer Chains near a Solid Interface. *ACS Macro Lett.* **2019**, 8 (8), 1006–1011. https://doi.org/10.1021/acsmacrolett.9b00351.

56 Pham, J. Q.; Green, P. F. The Glass Transition of Thin Film Polymer/Polymer Blends: Interfacial Interactions and Confinement. *J. Chem. Phys.* **2002**, 116 (13), 5801–5806. https://doi.org/10.1063/1.1456035.

57 Fryer, D. S.; Nealey, P. F.; de Pablo, J. J. Thermal Probe Measurements of the Glass Transition Temperature for Ultrathin Polymer Films as a Function of Thickness. *Macromolecules* **2000**, 33 (17), 6439–6447. https://doi.org/10.1021/ma0003349.

58 Fryer,D. S., Peter, Kim, E. J., Tomaszewski J. E., de Pablo, J.J., Nealey, P.F., White, C.C., Wu, W. L. Dependence of the Glass Transition Temperature of Polymer Films on Interfacial Energy and Thickness. *Macromolecules* **2001**, 34, 5627

59 Dequidt, A.; Long[a] D.R., Sotta P., Sanseau, O., Mechanical properties of thin confined polymer films close to the glass transition in the linear regime of deformation: Theory and simulations Eur. Phys. J. E (2012)35:61 DOI 10.1140/epje/i2012-12061-6

60 Wunderlich B., Macromolecular Physics, Academic Press, New York, 1976, Vol. 2, Ch.7.